Transverse-pumping approach for a powerful single-mode Ti:sapphire laser for near infrared lidar applications

Hannes Vogelmann,* Johannes Speidel, Matthias Perfahl, and Thomas Trickl

Karlsruhe Institute of Technology, IMK-IFU, Garmisch-Partenkirchen, Germany
**Corresponding author: vogelmann@kit.edu*

We present a design of a transversely pumped and powerful Ti:sapphire laser, suitable for laser remote sensing in the near infrared (NIR) spectrum. Examining multiple pump configurations revealed that transversal pumping of Ti:sapphire crystals with a Nd:YAG laser (532 nm) from one or two sides yields maximum output power. Together with an optimized bow-tie resonator setup, we were able to extract up to 3 W (30 mJ, 100 Hz) of narrowband NIR laser emission from a cuboid 50 mm long Ti:sapphire crystal. Beam quality and divergence were determined as $M_x^2 = 1.1$, $M_y^2 = 1.7$, $\varphi_x = 0.5$ mrad, and $\varphi_y = 0.8$ mrad. The spectral purity (seeded, $P_{\text{seed}} \geq 170$ μW) was better than 99.8%. Additionally, we show a two-wavelength setup applicable to atmospheric water vapor lidar. The prin-ciple performance of this theory of operation suggests a good chance of scalability towards significantly enhanced power of future Ti:sapphire lasers.

1. INTRODUCTION

Since its introduction as a laser medium for near infrared (NIR) laser emission by Moulton [1], titanium sapphire (Ti:Sa) has become a "rising star" [2]. Its initial low efficiency, caused by broadband absorption covering the spectral range of the laser emission by $Ti^{4+} - Ti^{3+}$ pairs [3], has quickly been overcome by improved methods of crystal growing. Ti:Sa lasers are the most common workhorses for both NIR tunable lasers and ultra-short pulse laser applications. This is particularly due to their extraordinary large fluorescent bandwidth, reaching from 760 to 1178 nm [4], which is ideal for replacing dye lasers in this spectral region with all the benefits of a solid state laser. The broad absorption range of Ti:Sa spans from roughly 450 to 600 nm with the maximum absorption around 500 nm.

For the pulsed excitation of Ti:Sa crystals, different methods have been applied so far. Most commonly used is laser radiation from pulsed Nd:YAG or Nd:YLF lasers, irradiated along the optical axis of the Ti:Sa crystal. Although the less intricate way of pumping Ti:Sa crystals laterally by direct excitation with flashlamps or light emitting diodes (LEDs), without a complex laser system in between, appears to be preferable, both are rather ambitious due to the relatively short fluorescence lifetime of only 3.1 μs [5]. Another issue is the non-isotropy of Ti:Sa, which allows optimum conversion efficiency only for a certain orientation of the polarization.

While flashlamp pumping of Ti:Sa was considered from the beginning ([6], e.g.), successful direct pumping of Ti:Sa with LEDs was first reported about 25 years later and is still under development ([7], and references therein). However, this approach is still limited by the short lifetime of the upper laser state of Ti:Sa, which does not allow for storing a large portion of energy delivered from LEDs as they still have a limited peak power. Thus, the output energy was confined to 32 μJ, and the reported conversion efficiency was only about 0.15% [8].

In contrast, flashlamp pumping of Ti:Sa in principle allows for generating high-power NIR pulses [9,10]. But, a major technical issue with flashlamp pumping is also essentially caused by the short fluorescence lifetime of Ti:Sa, resulting in rather low efficiency (<2%). Generating high-power pump pulses of appropriate lengths with flashlamps requires a very high peak current at a high voltage, leading to a comparatively high plasma temperature and a rather short life cycle due to the very fast erosion of the lamp electrodes. Furthermore, the emitted radiation shifts towards shorter wavelengths, where the conversion efficiency of Ti:Sa is significantly lower, and the degeneration of the Ti:Sa crystal by forming absorption centers ($Ti^{4+} - Ti^{3+}$ pairs) in its volume becomes likely ([9], and references therein).

Nevertheless, the only powerful all-solid-state flashlamp-pumped Ti:Sa laser with a certain appropriateness for long-term operation (flashlamp life cycle ≈ 10 million shots) was presented by Hoffstädt in 1997 [9]. It delivered up to 4.2 J in broadband operation. This system was upgraded to industrial standards by *ELIGHT* and was delivered to IMK-IFU (part of the Karlsruhe Institute of Technology) at Garmisch-Partenkirchen, Germany. It served as the powerful radiation source in water vapor differential absorption lidar (DIAL) and

was successfully used for atmospheric studies for more than 10 years [10–17]. This laser delivered up to 250 mJ at 800 nm in injection-seeded single-longitudinal-mode (SLM) operation [10], a value that has never been achieved by laser-pumped SLM Ti:Sa lasers with a single rod. The maximum pump energy of 235 J at the highest repetition rate of 42 Hz corresponded to an enormous average pump power of roughly 9.8 kW. Despite the low efficiency of this system, the maximum energy stored inside the rod was calculated to about 1.1 J [9], from which, with optimized volume matching, a possible extraction of about 0.7 J of single-mode radiation was estimated. The ability to store these high portions of energy is due to the large volume reached by the pump light from the source located along the sides of the extraordinarily long (150 mm) rod. This basic consideration and technical problems with the high flashlamp voltage (>25 kV), in combination with the degeneration of the Ti:Sa rod by ultraviolet light from the flashlamps, motivated the work described in this paper: the development of a new Ti:Sa laser transversely pumped with a frequency doubled Nd:YAG laser.

Because of the technical issues mentioned above, Ti:Sa excitation by "longitudinal" laser pumping along the optical axis of the Ti:Sa rod is the state-of-the-art technology. Initially, argon ion lasers were used for exciting the fluorescence, but have in the meantime been replaced by more powerful and reliable frequency doubled Nd:YAG or Nd:YLF lasers at 532 and 523 nm, respectively (e.g., [18–21]).

NIR lidar systems examining the short-term variability of the atmospheric state, such as water vapor distribution, require short averaging times and, thus, powerful NIR laser transmitters (e.g., [11,15,22–24]). Ti:Sa lasers have become the premier choice in the water vapor DIAL technique. Longitudinally pumped laser systems used so far have delivered pulse energies up to 150 mJ at low repetition rates [25]. For repetition rates of several hundred Hertz, stable lidar operation at average powers of up to 10 W have been demonstrated [23,26,27], this requiring a careful design and chilling of the laser crystals. An exception is the airborne DIAL of the German Aerospace Center (DLR) that takes profit of the low humidity at the cruising altitude [28–30]. Here, the substantially stronger 935 nm absorption band of the H_2O band can be used, which results in the possibility of DIAL measurements also in the lower stratosphere. Although Ti:Sa itself emits at these wavelengths too, optical parametric oscillators have been preferred by the DLR team.

Besides the proper choice of pumping sources, we assume the setup of the pumping geometry to be key in terms of stable, high-energy Ti:Sa emission. Longitudinally pumped lasers use a geometry that feeds the pump beam through one or both end faces of the crystal rod. With respect to a reasonable Ti^{3+}-doping, the rod's length is thereby typically limited to about 2 cm [31]. Thus, with a given diameter of the pumped volume, the amount of maximum storable energy is limited and demands "hot" pumping of a relatively small volume. By increasing the diameter of the pump beam, and in (last) consequence the diameter of the Ti:Sa rod, the amount of maximum storable energy could be further improved. However, this alteration leads to severe thermal problems. While conserving the laser gain, the pump energy is proportional to the cross section of the pump beam $A = d^2$, where d is the diameter of the pump beam. At the same time, the cooling capability of the barrel surface is proportional only to the diameter of the Ti:Sa rod. Therefore, the maximum output is limited by the risk of destroying the Ti:Sa crystal.

This limitation of longitudinal pumping can be avoided by transversely pumping Ti:Sa rods, which is the key advantage of our proposed setup. This is simply because the length of the rod is thereby not limited by the penetration depth of the pump light. This concept has already been chosen in the abovementioned flashlamp-pumped system of Hoffstädt [9] with its extraordinary large Ti:Sa rod. The mentioned setup by Pichon [8], using an LED as the primary light source also made use of direct, transverse pumping. Interestingly, to our knowledge, direct transverse pumping of Ti:Sa by lasers has never been deployed for lidar purposes.

However, with the recent development of commercially available, very powerful diode-pumped solid state (DPSS) lasers, performing up to 100 W at 532 nm, the pump energy for powerful Ti:Sa lasers became available. Considering the success with the lossy side-pumping with flashlamps that also emit outside the absorption band of Ti:Sa, transverse laser pumping becomes an interesting option. We assume it becomes mandatory if one aims at increasing the NIR output power of Ti:Sa lasers to a maximum.

In this paper, we present the concept of transversely pumped Ti:Sa rods using a Nd:YAG laser and show the experimental results. In Section 2, we discuss the relevant theoretical and geometrical considerations and describe basic pumping experiments with different geometrical setups. In Section 3, we show an optimized setup and its performance in a seeded bow-tie resonator that is suitable for the generation of narrowband NIR laser pulses with high spectral purity and sufficient pulse energy for remote sensing applications. In Section 4, we discuss the results achieved. Finally, in Section 5, we give conclusions and an outlook with respect to further development and improvements.

2. THEORETICAL CONSIDERATIONS AND BASIC EXPERIMENTS

It is well known that both the absorption cross section for polarized pump light and the intensity of NIR fluorescence of Ti:Sa strongly depend on the orientation of the crystal's c axis [5]. For optimal pumping efficiency, the c axis has to be parallel to the polarization of the pump light. The maximum fluorescence is observed within the same polarization as the c axis (π orientation). In the case of perpendicular orientation (σ) of the crystal's c axis, both pump light absorption and fluorescence are weaker by a factor of roughly 0.4 [5]. This must be considered in any Ti:Sa resonator design, regardless of its pump geometry.

The effective intensity P of pump light propagating inside a cylindrical or cuboid Ti:Sa rod at a certain location L can be calculated as a combination of the Beer–Lambert law and geometrical considerations:

$$P_L = \sum_i P_{iL}(z_i) = \sum_i P_{0i} \frac{f_i}{f_i - z_i} \gamma_i e^{-\alpha_\parallel \gamma_i z_i}. \quad (1)$$

The index i denotes a certain path of the pump light in the case of pumping from more than one side, z_i is the dedicated

path length inside the rod between the surface and the location of interest L, and P_{0i} is the pump light intensity of the ith pump beam at the crystal's surface. f_i denotes the focal length of the ith pump beam within the crystal, which means the distance from the surface of incidence to the area of focus (cylindrical optic). The effective absorption coefficient is simplified to $\alpha_{\parallel} \cdot \gamma_i$, where γ_i denotes an efficiency term that takes the anisotropy of Ti:Sa into account:

$$\gamma_i = \cos(\vartheta_i) + (1 - \cos(\vartheta_i))\frac{\alpha_{\perp}}{\alpha_{\parallel}}, \qquad \textbf{(2)}$$

where $\alpha_{\parallel}$ and $\alpha_{\perp}$ are the absorption coefficients for the polarization parallel and perpendicular to the c axis, respectively, and $\cos(\vartheta_i)$ accounts for the dependency on the angle ϑ_i between the orientation of the c axis and the polarization of the ith pump beam. If the c axis and the polarization of the pump light are parallel, $\cos(\vartheta_i)$ and γ_i equal one. In the worst case of perpendicular polarization, $\cos(\vartheta_i)$ and γ_i become zero and 0.4, respectively. For focal lengths f_i significantly longer than the pump beam diameter d_i, this is a useful approximation because $|\Delta\vartheta_i| \leq \arcsin(d_i/(2f_i))$. In the case of pumping a cylindrical Ti:Sa rod ($\varnothing = 10$mm, $n_S = 1.77$ at 532 nm) floating in water ($n_W = 1.33$), f_i becomes 20.1 mm (in air: $f_i = 11.5$ mm). Even for an 8 mm wide pump beam with the polarization parallel to the c axis, this means $\cos(\vartheta_i) \geqslant 0.98$. Therefore, in cases of pumping from one or two sides with optimal orientation of the c axis, γ_i is assumed to be one.

The term $f_i/(f_i - z_i)$ in Eq. (1) is a simplified geometry factor that does not take into account the waist of the pump beam close to its focal point, but that is useful if the focal point of the pump beam is located outside the rod. In the simplest case of a pump beam collimated inside the crystal, the geometry term equals one. Calculated effective pump light intensities for basic configurations are highlighted in Fig. 2.

The preferable geometrical configuration for transverse pumping should align the polarization of the pump light parallel to the c axis of the Ti:Sa crystal. This requires an alignment of the pump light in a plane perpendicular to the axis. Most fluorescence emission c from the crystal is then emitted with the same polarization and within the same plane (Fig. 1). This implicates that transverse pumping of cylindrical- (barrel) or cuboid-shaped rods, under maximum conversion efficiency, is reasonable only from two sides unless very high pump energy is available. As there is no transmission of pump light through the end faces of the rod in a transverse setup, it is preferable to rather use perpendicularly cut rods with a NIR anti-reflection (AR) coating than a Brewster cut. The latter would contribute additional absorption due to a "dead" volume, which cannot be reached by the pump light aligned perpendicular to the longitudinal axis of the rod.

Most commonly, laser rods are of cylindrical shape. Starting from the very long (152.4 mm) cylindrical rod of the flashlamp-pumped laser, we carried out most experiments with such rods. The rods tested are listed in Table 1. All rods but #7 (cuboid) are cylindrical. Except rod #1, all rods were purchased from Döhrer Elekrooptik. The manufacturer Crystal Systems claimed a figure of merit (FOM) larger than 300. This was verified by our own characterizing measurements of the absorption coefficients for the wavelength of the strongest fluorescence (800 nm) and

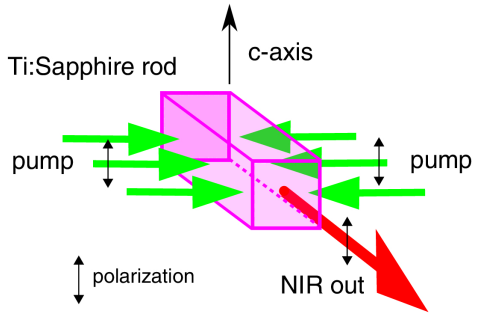

Fig. 1. Basic configuration for transverse pumping. The c axis of the Ti:Sa crystal is aligned parallel to the polarization of the pump light for optimal conversion efficiency.

the wavelength of the pump light (532 nm), α_{800} and α_{532}, respectively. This was done for polarization both parallel and perpendicular to the crystal's c axis (Table 1, #2–#7). The FOM was calculated as the ratio of α_{532} and α_{800} in parallel polarization. For comparison, we also characterized rod #1 (used rod from our flashlamp-pumped system, manufacturer: Union Carbide) which showed a significant lower FOM, presumably due to its long use ($\approx$ 100 million shots).

For the experiments described in this section, we used a Powerlite 8020 Precision Nd:YAG laser from Continuum in unseeded operation that delivered 300 mJ at 532 nm and 20 Hz repetition rate. This was the highest pulse energy available to us at that time.

As the first experiment, we transversely pumped a cylindrical rod (#2 in Table 1, spare part from our flashlamp-pumped Ti:Sa system) from one side through its rough barrel face with an appropriately expanded beam. With an optimally aligned orientation of the crystal's c axis parallel to the vertical polarization of the pump light, we were able to extract 7 mJ of NIR broadband ($\approx$ 800 nm, spectrum not determined) laser emission from a linear Fabry–Perot resonator setup with an 85% output mirror.

One general trade-off using cylindrical rods became already apparent in this first experiment. Pumping through the cylindrical barrel face deflects the outer parts of the pump beam towards the crystal axis and, thus, excites just a small fraction of the crystal volume. Furthermore, this refraction comes along with pump light that is partly no longer polarized exactly parallel to the c axis, depending on both the beam diameter of the pump light and the radius of the barrel.

This issue could principally be solved by using a cuboid rod. For achieving an optimum gain homogeneity of the pumped volume in a cuboid rod, we calculated that the pump light should incline with a small angle of convergence due to the absorption losses inside the crystal. For a 7 mm wide cuboid rod with 0.1% doping, this means a reduction of the pump beam diameter by 30% from the surface to the other side of the rod. This corresponds to a focal length of 23.3 mm, which is very close to the focal length of the pump beam inside a cylindrical rod under water (20.1 mm). However, this results in an unused fraction of the crystal volume of at least 15% if the pumping is conducted from two sides. Different courses of the pump light intensity throughout the cross section of cylindrical and cuboid Ti:Sa rods are shown in Fig. 2.

Table 1. Absorption Coefficients α_{800} and α_{532} for 800 nm and 532 nm, Respectively, Calculated from Measured Transmissions T_{800} and T_{532} for These Wavelengths

Technical Specifications of Laser Rods												
#	Shape	Dimensions [mm]	Doping [%]	α_{800} [cm^{-1}]		T_{800}		α_{532} [cm^{-1}]		T_{532}		FOM
				$\parallel c$	$\perp c$	$\parallel c$	$\perp c$	$\parallel c$	$\perp c$	$\parallel c$	$\perp c$	
1	Cylinder	152.4 × 10	0.10	0.0066	0.0138	0.90	0.81	1.46	0.79	$\leq 10^{-9}$	$7 \cdot 10^{-6}$	221
2	Cylinder	152.4 × 10	0.10	0.0029	0.0041	0.96	0.94	1.46	0.72	$\leq 10^{-9}$	$1.9 \cdot 10^{-5}$	469
3	Cylinder	152.4 × 10	0.07	0.0021	0.0033	0.97	0.95	1.01	0.65	$2.7 \cdot 10^{-7}$	$5.5 \cdot 10^{-5}$	481
4	Cylinder	100 × 10	0.07	0.0024	0.0041	0.99	0.96	1.39	0.59	$9.7 \cdot 10^{-7}$	$3.0 \cdot 10^{-3}$	579
5	Cylinder	50 × 10	0.07	0.0035	0.0047	0.99	0.98	1.45	0.77	$6.9 \cdot 10^{-4}$	$2.1 \cdot 10^{-2}$	414
6	Cylinder	50 × 10	0.10	0.0029	0.0041	0.97	0.96	1.46	0.72	$6.8 \cdot 10^{-7}$	$2.7 \cdot 10^{-4}$	469
7	Cuboid	50 × 7 × 7	0.10	0.0029	0.0041	0.97	0.96	1.46	0.72	$6.8 \cdot 10^{-4}$	$2.7 \cdot 10^{-2}$	469

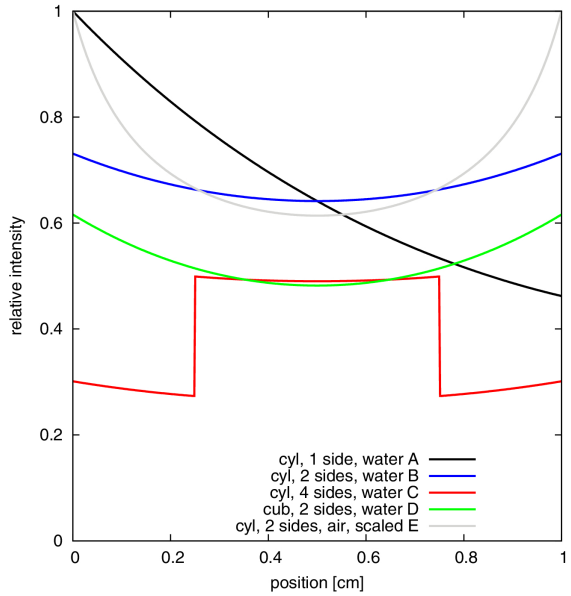

Fig. 2. Relative intensity of the pump light inside cylindrical (cyl) or cuboid (cub) Ti:sapphire crystals (width 1 cm, doping level 0.1%) as a function of the transverse position in the case of pumping from one, two, or four sides. The pump intensity of an 8 mm wide pump beam from one side containing the entire pump power at the surface of the rod is set to one (except E). For A, B, D, and E, the c axis is parallel to the polarization of the pump light. In the case of pumping from two or four sides the intensity contributed by each path is 1/2 or 1/4 of the entire power, respectively. Pumping the cylindrical rod embedded in water shows a significant drop of intensity if pumped from one side (A) and a much more homogeneous intensity if pumped from two sides (B). In the Bethune configuration with four pump beams and an angle of 45° between the c axis and polarization of each pump beam, the effective pump light intensity is significantly lower, even in the central volume where all pump paths overlap (C). Pumping a cuboid rod with a collimated beam (D) from two sides shows a larger variation of the intensity compared to the focused case (B, focal length 20.1 mm). Pumping a cylindrical rod in air (focal length 11.5 mm) from two sides (E, scaled to one for comparison) also shows a larger variation of intensity compared to pumping in water (B).

To illuminate a larger fraction of the crystal's volume, we attempted both diffuse pumping and side pumping in a Bethune setup [32]. This configuration is known from some dye lasers aiming at better beam quality and lower frequency chirping [33,34]. However, this is a trade-off at the expense of the optimal orientation between polarization and c axis. For achieving an optimum spatial homogeneity of the laser gain in a Bethune setup, the c axis has to be oriented 45° against all four incident pump light directions. Therefore, for a given overall pump power, the effective pump light intensity in the central volume (best overlap) is significantly reduced compared to pumping from two sides with optimal orientation of polarization and c axis (Fig. 2). And, we were not able to generate NIR laser emission from a Ti:Sa rod in this configuration.

The side faces of the Ti:Sa rods are micro ground with a certain roughness to avoid transverse lasing inside. This leads to some diffusion of the pump light traveling through the ground surface, but still sufficiently conserves its polarization and direction. The diffusion is smaller if the crystal is embedded in water due to better phase matching at the rough surface.

It turned out that transversely pumping an only 40–70 mm long fraction of the rods yielded the maximum NIR output. This indicated a significant lack of pump energy in this setup for the longer rods (Table 1, #2, #3, #4) if transversely pumped along their entire volume. Thus, different basic setups of transverse laser pumping have been examined in a Fabry–Perot resonator setup with a 50 mm long Ti:Sa rod (Table 1, #5). For some experiments, the rod was embedded in water inside a water-filled glass tube with an AR coating. This allowed for better refractive index matching and sufficient cooling and, therefore, led in a later implementation to the use of an operational pump chamber with water flow. All experiments were carried out with a plane-parallel resonator featuring an 85% output coupler (OC). To match the length of the Ti:Sa rods, the pump beam was horizontally expanded to 45 mm with a plano–concave cylindrical lens ($f = -400$ mm) while conserving its vertical diameter of 8 mm. To avoid damages of the rods by self-focusing, the pump energy was reduced to 230 mJ in some configurations. Details are noted below.

(1) Pumping a cylindrical rod from one side without embedding in water (dry). With an optimal alignment of the crystal's c axis, an output of 10 mJ was obtained at a pump energy of 210 mJ. The output increased to 18 mJ at a pump energy of 230 mJ. The laser threshold in this setup was determined at a pump energy level of 185 mJ. The fluorescent volume shows a triangular cross section due to the refraction of the pump light at the cylindrical face of the

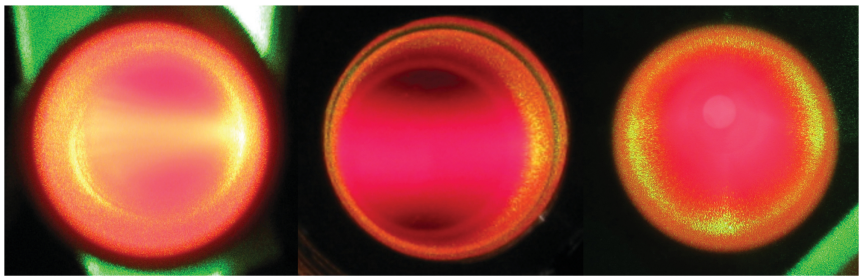

Fig. 3. Shape of the fluorescent area viewed through the front face of a cylindrical Ti:sapphire crystal (Ø = 10 mm). Pumping in air from one side (left), under water from two sides (middle), and under water from four sides in Bethune configuration (right). The observed laser emission was related to the fluorescent volume except the Bethune configuration (no laser emission was observed).

crystal (Fig. 3, left). A misalignment of the crystal's *c* axis to 15° drastically reduced the output by 80%.

(2) Pumping a dry cylindrical rod in a spectralon diffusion chamber as in the flashlamp-pumped laser system [9,10]. This setup did not result in any laser emission even with a pump energy of 300 mJ. This had been expected because of losses in the spectralon. Also, the depolarized diffusely scattered light inside the chamber matches the optimum polarization parallel to the crystal's *c* axis only with a fraction of 50%.

(3) Pumping a dry cylindrical rod from four sides in a Bethune setup (i.e., [32]). No NIR laser emission was observed in any alignment of the crystal's *c* axis at a pump energy of 300 mJ. The fluorescent volume showed a rather homogeneous cross section, similar to the pumping while floating in water (item 4, Fig. 3, right).

(4) Pumping a floating cylindrical rod in a Bethune setup. No NIR laser emission was observed in any alignment of the crystal's *c* axis at a pump energy of 300 mJ. The fluorescent volume showed a rather homogeneous cross section with a wide utilization of the entire crystal volume (Fig. 3, right).

(5) Pumping a dry cylindrical rod from two sides with 230 mJ (115 mJ each) yielded 15 mJ of NIR laser emission, which is somewhat weaker than the value observed for pumping from one side (item 1). The fluorescent volume showed a rather narrow beam shape along the rod's cross section.

(6) Pumping a floating cylindrical rod from two sides with 230 mJ (115 mJ each) yielded 21 mJ of NIR laser emission. The higher exploitation is presumably the result of better refractive index matching at the barrel surface. The fluorescent volume showed a timber-like cross section, but with a larger extent as seen in the dry setup without water. A significant dark fraction of the entire volume of the crystal remained, which is a significant difference from the Bethune setup (Fig. 3, middle). Less than 50% of crystal volume is illuminated by the pump light.

As sufficient pump power was available only for 50 mm long rods and a higher doping level was expected to gain conversion efficiency, one of the cylindrical rods (Table 1 #2, doping level 0.1%) was sent back to the manufacturer and cut into 50 mm long pieces. One of these pieces was left cylindrical (Table 1, #6) while another piece was ground into a cuboid shape (Table 1, #7). Both rods were repolished, and a new AR coating was added. As stated above, from the plain sidewalls of the cuboid rod, a better parallelism of the pump light's polarization to the *c* axis and therefore higher conversion efficiency was expected.

As two-sided pumping performed best in the basic experiments, both the cylindrical rod (Table 1, #6) and the cuboid rod (Table 1, #7) were mounted in operational pump chambers (manufactured by Radiant Dyes) with a continuous temperature-stabilized water flow and AR windows with reduced coupling losses. From the higher doping rate of these rods (0.1%), we expected better conversion efficiency with a reasonable extinction of the pump light. The short path lengths transverse the rods of only 10 mm (cylindrical) and 7 mm (cuboid), and the absorption cross section $\alpha_{532} = 1.46\,\mathrm{cm}^{-1}$ leads to absorptions of the pump light of 77% and 64%, respectively. Both rods (Table 1, #6, #7) were bonded into stainless steel hulls with silicone at both ends for fixation in the pump chambers.

The cylindrical rod (Table 1, #6) was pumped from two sides with quasi-collimated beams (1.5 mm × 45 mm, 115 mJ each), widened horizontally, and focused vertically with cylindrical lenses (−30 mm, 400 mm). An output of 37 mJ was obtained in a linear resonator setup with an OC of 72%. This marks a significant gain with respect to the formerly achieved 21 mJ in the basic experiment no. 6.

3. APPLICATION IN AN OPERATIONAL LASER SYSTEM

After determining the optimal configuration for transverse pumping, an appropriate resonator configuration fulfilling the requirements for narrowband seeding with two wavelengths had to be defined. The traveling wave bow-tie resonator configuration is well established and has been used in many applications after its introduction (e.g., [35]). Following the principal configuration by Ertel *et al*. [36] and some further improvements introduced by Metzendorf [26], a one-stage powerful oscillator in a bow-tie configuration was implemented (Fig. 4). The basic resonator setup, consisting of three highly reflective mirrors and one OC, was supplemented by a Faraday rotator and a half-wave plate to allow for only one direction of light circulation inside the resonator. Polarizing prisms, which are commonly used in combination to form a Faraday isolator, were not used due to their low damage threshold and the sufficient polarization dependency of amplification in the Ti:Sa crystal. To suppress the amplification of spontaneous emission (ASE) near the spectral gain maximum at about 800 nm, a tunable Lyot filter with three

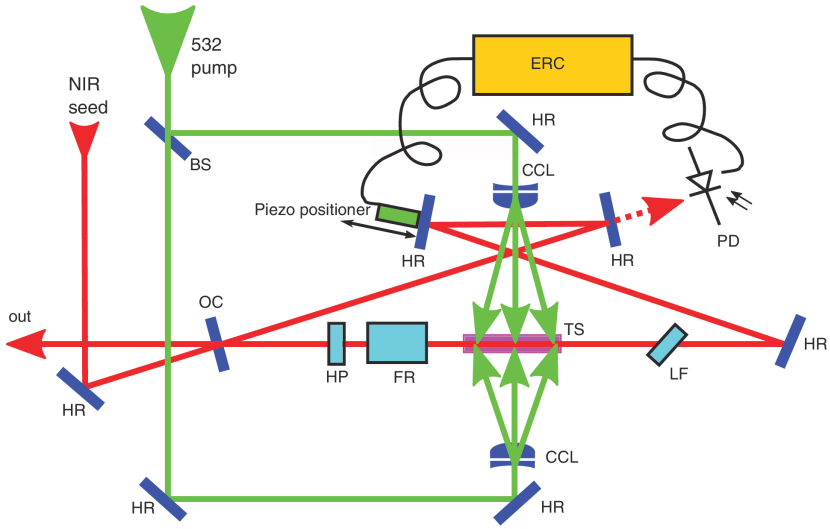

Fig. 4. Powerful and compact "bow-tie" resonator configuration for the generation of narrowband NIR laser pulses. The crossed cylindrical lenses (CCL) widen the pump beams horizontally to 45 mm and narrow it to about 1.5 mm vertically. TS, Ti:Sa rod; BS, beam splitter; HR, highly reflective mirror; OC, output coupler; HP, half-wave plate; FR, Fresnel rhomb; LF, Lyot filter; PD, photodiode; ERC, electronic resonance control.

birefringent plates (thickness 990 μm, each) made out of quartz was placed inside the resonator with an incidence angle of 57° (Brewster angle). For fine tuning of the resonator length, one mirror was mounted on a piezo translator. Together with all optical components, mounts, housings, and further mechanical restrictions, the resonator was set up with an overall length of 1.40 m.

For this configuration, a new diode-pumped, injection-seeded Nd:YAG laser was used (Innolas, EVO III). This laser runs at a much higher repetition rate (100 Hz) and delivers 250 mJ pulses at 532 nm. Each pump beam was horizontally widened almost to the length of the Ti:Sa rod (50 mm) and vertically narrowed to 2 mm with a pair of crossed cylindrical lenses (CCL in Fig. 4). Using the pump chamber with cylindrical rod #6 (Table 1), a maximum output of 18 mJ was extracted from this resonator at a pump level of 250 mJ (OC of 85%). Surprisingly, the cuboid rod (Table 1, #7) did not result in a higher output in exactly the same configuration. The maximum output of 17 mJ was even weaker. The slightly higher output from the cylindrical rod was presumably caused by the refraction of the pump light towards the center of the rod, leading to a smaller illuminated volume, but with a higher gain. This effect seems to be stronger than the loss of efficiency caused by the polarization that is partly no longer parallel to the c axis of the Ti:Sa crystal. The laser threshold for this two-sided pumping was determined at a pump level of 88 mJ from each side. To increase the laser gain in the pumped volume of the crystal, the cuboid rod was finally pumped from only one side with the entire available pump energy of 250 mJ. The vertical focus of the pump beam (cylindrical lens, $f = 400$ mm) was successively moved towards the Ti:Sa rod. This was continued until a bulk damage of the crystal occurred when the vertical focus reached the opposite side of the Ti:Sa crystal. Before reaching the damage threshold, the highest possible NIR output obtained in a stable long-term operation was 27 mJ (OC of 75%). Moving the vertical focus further towards the rod yielded a short-term output of roughly 30 mJ, but with a risk of damage. We assume that the maximum possible output could have been even higher with an optimized convergence of the pump beam as described above. All further applications were carried out with this rod (Table 1, #7) in undamaged parts of its volume.

Different OCs (60%, 70%, 72%, 75%, 80%, 85%) were tested for maximum output from the cuboid rod. Two-sided pumping with two quasi-collimated beams led to a smaller gain from a larger volume. In this case, the highest possible output was 1.8 W using an OC with a reflectivity of 85%. The highest output of 3.0 W (30 mJ) was achieved with the 75% OC while transversely pumping from one side. As known from other high-power Ti:Sa lasers in a comparable resonator setup, highest outputs were achieved with 60% OCs. To our understanding, this means that the pumped volume, which is comparatively large in our setup, is less excited.

A. Two-Wavelength Seeding

For its purpose as a laser transmitter in a water vapor DIAL system, two NIR wavelengths need to be transmitted at almost the same time. Together with Radiant Dyes, a concept of seeding and resonance control using analog computing was developed. The pump laser operates with a repetition rate of 100 Hz while both continuous wave (cw) seeding wavelengths are coupled into the resonator in alternating sequence. The principal concept is the stabilization of the resonator to the first wavelength (λ_{on}), while the second wavelength (λ_{off}) is adapted to the given resonator length defined by λ_{on}.

The resonance of the current seeding wavelength is detected by a photodiode behind one resonator mirror, while the position of another resonator mirror is wobbled with a piezo positioner (Fig. 4) driven with a sine of 200 Hz, which is twice the repetition rate of the laser system. The amplitude of this sine is chosen in a way that the free spectral range (FSR) of the resonator is fully covered at least once. Thus, a resonance for the actual wavelength is detected and sampled at least once during the rising

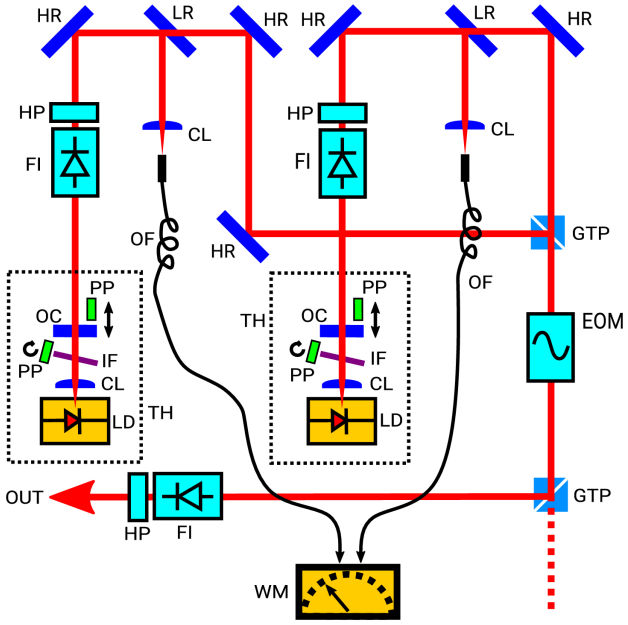

Fig. 5. Configuration of the seeding device with two NIR output wavelengths. Each laser diode (LD) is operated inside a temperature controlled housing (TH). An external cavity configuration is formed by a collimating lens (CL), a tunable interference filter (IF) with piezo positioner (PP), and an output coupler (OC) with piezo positioner (PP). The NIR output from each cavity passes a Faraday isolator (FI) and a half-wave plate (HP) for protection against back reflections. The left diode laser is *s* polarized, while the right diode laser is *p* polarized with respect to the following mirrors (HR and LR) behind the half-wave plates (HP). A small fraction of each emission is coupled into an optical fiber (OF) and measured by a wavelength meter (WM, High Finesse, WS7) with an upstream multiplexer device. The two beams with different wavelengths and crossed polarization are combined in a Glan–Thomson prism (GTP). Switching between the two wavelengths is finally executed by passing the combined beams through an electro optical modulator (EOM), which is modulated with a square wave at half-wave voltage followed by a second GTP.

slope of the sine modulating the resonator length. To avoid dazzle and disturbing signals, sampling is enabled electronically only during the rising slopes in which the pump laser is not fired, and the resonator is not emitting NIR. The timing sequence of the resonance control is shown in Fig. 5. The resonator length is adapted to λ_{on} by measuring the time between the first zero crossing of the piezo driving sine t_0 and the resonance signal from the photodiode. With a sample and hold circuit and a proportional–integral–derivative controller (PID) controller, an offset is added to the sine in a way that the time of the resonance signal is as close to t_0 as possible. In a second step, wavelength λ_{off} is adapted to the given resonator length in the same manner, using a second sample and hold circuit and a second PID controller connected to the temperature control unit of the second diode laser to tune its wavelength. In consequence, the control of the resonance of the second seeding wavelength λ_{off} is linked to the adjustment and stability of λ_{on}. This could be a drawback for certain applications. In the case of an atmospheric DIAL for water vapor, this is no constraint if the second wavelength is used as "λ_{off}."

The two seeding wavelengths are generated by two widely tunable external cavity diode lasers. Their functional principle [37] is based on a low-loss interference filter inside the cavity and, thus, different from the common wavelength selection with a grating (e.g., [38]). The technical implementation of the diode lasers and the switching between both wavelengths with an electro-optical switch (Fig. 6) was developed by Radiant Dyes. The seed lasers show already a great passive long-term stability (several hours) of their wavelengths by their accurate temperature control (within ±0.0003 nm). Using the built-in feedback loop of the employed wavemeter (High Finesse WS7), the stability is limited by the accuracy of the wavemeter (±0.00001 nm). The maximum output powers of the diode lasers are 55 and 65 mW. After passing all optics, about 13 and 15 mW reach the OC of the Ti:Sa laser resonator. This is far beyond the seeding threshold for a perfectly adjusted beam overlap. A stable lock into seeding was observed above 170 μW at the OC.

4. RESULTS AND DISCUSSION

The transversely pumped Ti:Sa laser was characterized in its final setup, and mounted in the ATMONSYS (Atmospheric Monitoring System) lidar system of IMK-IFU inside a transportable cargo container. A beam divergence of 0.8 mrad × 0.5 mrad and a pointing stability better than 0.1 mrad were measured by directing the beam to a target at a distance of 25 m. The beam quality parameters $M_x^2 = 1.1$, $M_y^2 = 1.7$ and relative beam waist astigmatism of 14% were measured by focusing the beam with a plano–convex lens ($f = 250$ mm) in combination with a CCD camera mounted on a motorized driving stage (Fig. 7). The beam profile is close to an elliptic Gaussian (2.4 mm/1.4 mm), but slightly asymmetric in x direction (embedded in Fig. 7). This is presumably caused by the asymmetric transverse pumping from only one side in this setup.

The spectral purity of the emitted NIR laser pulses is conservatively estimated to at least 99.8%. This is close to the findings of Ertel *et al*. [36] who determined a spectral purity of 99.97% in a comparable configuration and fulfills the requirement of DIAL operation [39].

The spectral purity was determined by measuring the extinction of the NIR radiation by water vapor in the spectral range from 817.1825 to 817.2868 nm, which contains a strong water vapor absorption line ($\sigma = 41.2\ \mathrm{cm}^{-1}\ \mathrm{molecule}^{-1}\ \mathrm{cm}^2$ [40]). For this purpose, a nearly 20 km long quasi-horizontal path was used by recording the lidar return from a snow covered mountain slope at a distance of 9.7 km. From the atmospheric conditions during this experiment (10°C, ≈80% relative humidity), one would by far expect a saturated extinction at the line center (Fig. 8). Thus, only lidar return due to spectral impurity could be recorded at this wavelength. We assume that the spectral purity could be further improved by taking care of an optimized matching of the beam profile of the seeding radiation and the cross section of the pumped volume.

By spectral analysis with a confocal etalon (FSR of 1.5 GHz, $\mathcal{F} = 200$), the bandwidth of seeded laser pulses from the Ti:Sa laser was estimated to be not significantly larger than the specified bandwidth of the etalon of 7.5 MHz. This is

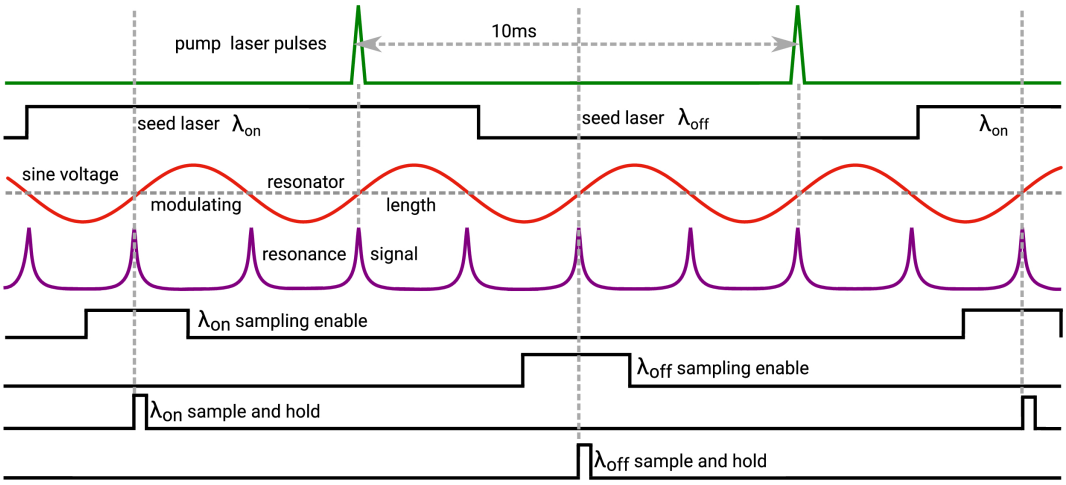

Fig. 6. Timing diagram of the resonator and seeding control. The laser is firing at a repetition rate of 100 Hz, while the resonator is modulated with a 200 Hz sine. Sampling of both λ_{on} and λ_{off} resonance signals is enabled only during the ascending slope of the modulating sine and while the laser is not firing. The sample and hold signals of both seeding wavelengths are fed into a PID controller, each targeting to keep the sample and hold signal close to zero crossing of the ascending slope of the sine. This ensures a resonant state of the resonator for the respective wavelength during the following zero crossing of the ascending slope sine when the laser is fired. The vertical dashed lines mark the time of resonance sampling and firing. The dashed horizontal line marks the zero level of the sine.

in some agreement with the transform limit of 8.8 MHz for Gaussian pulses with a duration of 50 ns. The pulse shape is close to a Gaussian with a slight asymmetry and does not show a significant mode beating (Fig. 9).

As part of the ATMONSYS lidar system, the transversely pumped Ti:Sa laser was extensively tested during the CHEESEHEAD (Chequamegon Heterogeneous Ecosystem Energy-Balance Study Enabled by a High-Density Extensive Array of Detectors) [41] and FESSTVaL (Field Experiment on Submesoscale Spatio-temporal Variability in Lindenberg) [42] field campaigns.

The resonator and its electronic and opto-mechanical control turned out to be basically stable for continuous operation with an average power up to 2.7 W NIR, corresponding to a pulse energy of 27 mJ. In this setup, only a small fraction (<20%) of the volume of the cuboid rod (7 mm × 7 mm × 50 mm) was pumped. With a more powerful pump laser, allowing for a more effective pumping of a larger volume, this should be scalable up to a volume fraction of approximately 85% if using two slightly convergent pump beams (2 × 450 mJ) conserving a homogeneous pump intensity throughout the volume (Section 2). Thus, an NIR output of about 110 mJ could be expected from this rod in this configuration. This is roughly consistent with the maximum output of 250 mJ achieved with our former flashlamp-pumped Ti:Sa laser with a 150 mm long rod [10].

The satisfactory NIR laser output of more than 2 W was achieved by pumping only from one side, resulting in a slightly asymmetric beam profile. On the other hand, pumping from one side reduced the optical elements, the expense for adjusting,

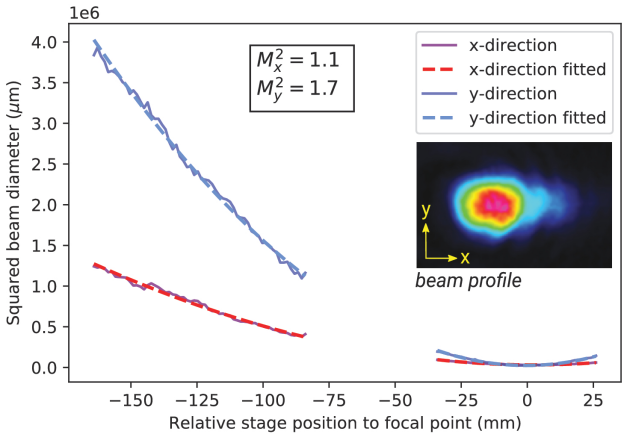

Fig. 7. Beam quality parameter M^2 was determined to $M_x^2 = 1.1$ and $M_y^2 = 1.7$ with a CCD camera driven along the focal point of the ray behind a plano–convex lens ($f = 250$ mm). Due to the high intensity near the focal point, the measurements within the Rayleigh length were recorded separately with a stronger OD filter. The beam profile is elliptic (2.4 mm; 1.4 mm) and close to a Gaussian, but slightly asymmetric in x direction.

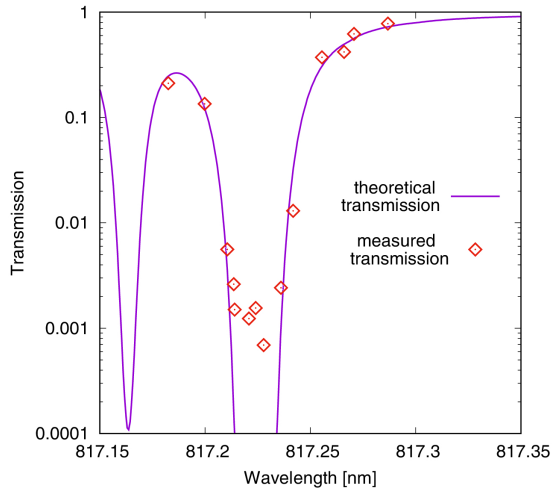

Fig. 8. From a transmission measurement with a rather horizontal 20 km path length in a humid atmosphere (900 mb 10°C, 80% RH), we estimated a spectral purity larger than 99.8%.

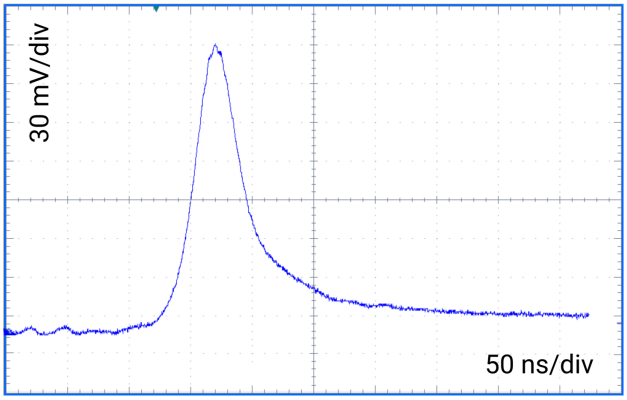

Fig. 9. Pulse shape of the seeded Ti:sapphire laser is close to a Gaussian with slight asymmetry and without significant mode beating. The pulse duration (FWHM) was determined to 50 ns.

and the required space to a minimum while the stability of the whole setup was increased.

In this configuration, the efficiency might be enhanced by using a cuboid rod with one polished side face to achieve better conservation of the polarization of the pump light, which has not been tested yet. However, two polished side faces could lead to undesirable effects, such as transverse laser modes inside the rod.

Since the laser system is assembled inside an air-conditioned container designated for field campaigns, the initial performance of single-mode operation was insufficient. After some improvements (removal of the air-conditioning compressor and implementation of an actively stabilized and air damped laser table), a reasonable stability for operational atmospheric lidar soundings was achieved.

5. CONCLUSION

For ground-based lidar measurements of water vapor covering the entire troposphere, very high power is needed to overcome the considerable signal limitations. In addition, short measurement times are mandatory because of the high variability of the lower atmospheric humidity. From the results obtained in this study, we conclude that the method presented has great potential for more powerful Ti:Sa lasers in the future. This is a consequence of the comparatively large surface hit by the pump light and the advantageous proportion of a cooled surface and pumped volume. This allows for a significant higher average pump power than the values achieved within this work for the given crystal geometries.

If the pump power is not a limiting factor, the Bethune configuration could be most promising toward the highest possible output, because of the optimum fraction of homogeneously pumped volume, but with the drawback of low conversion efficiency due to the 45° tilt of the c axis relative to the polarization of the pump light from all four directions. So far we have not been able to demonstrate any laser emission from a Ti:Sa crystal pumped in a Bethune setup.

The different investigated pump configurations have shown that pumping from two sides or even from only one side with π orientation is most promising for high laser output with reasonable efficiency. From theoretical considerations, we conclude that using cuboid rods should yield better conversion efficiency and better exploitation of the crystal volume.

Compared to conventional longitudinally pumped Ti:Sa lasers, transverse pumping reveals a great robustness of the pump beam alignment. The omission of dichroic mirrors in the resonator due the complete separation of pump light and laser emission pathways is also an obvious advantage in comparison with longitudinally pumped Ti:Sa lasers.

As the minimum level of power for stable seeding turned out to be as low as 200 μW, seeding stability could be improved significantly by using fibers instead of long beam paths on the laser table. This is an important aspect for a laser system used in field campaigns outside the laboratory.

As further steps towards an optimized configuration, slightly higher doping levels of employed Ti:Sa crystals should be considered. With a crystal of the size we used (7 mm × 7 mm × 50 mm), higher output should be scalable with higher pump energies up to a factor of about five. Even an average pump power of more than 100 W should not lead to a cooling problem with a rod of this size flushed in water. In summary, by the method of transversely pumping Ti:Sa crystals, the prospects for major improvements of pulsed high-power and narrowband NIR laser transmitters, as used in lidar remote sounding, are substantial.

Funding. Bundesministerium für Wirtschaft (KF2371502); Helmholtz Association; Deutsche Forschungsgemeinschaft (406980118); Karlsruhe Institute of Technology.

Acknowledgment. We thank Ankur Desai (University of Wisconsin, Madison) and Matthias Mauder (Karlsruhe Institute of Technology) for inviting us to take part in the CHEESEHEAD project; Simon Metzendorf (University of Hohenheim) for practical hints for the implementation of the Lyot filter; and Mart Rahkema and the late Aivo Reinart † (Radiant Dyes Laser) for permanent support with the ongoing development of the laser resonator control electronics. The cooperation with Radiant Dyes Laser was funded by the Bundesministerium für Wirtschaft within the program "Zentrale Innovation Mittelstand" (ZIM). The development of the mobile ATMONSYS lidar was funded within the project ATMONSYS (Atmospheric Monitoring System) by the HGF. The participation within the project CHEESESHEAD (Chequamegon Heterogeneous Ecosystem Energy-Balance Study Enabled by a High-Density Extensive Array of Detectors) was funded by the DFG. Beyond third party funding, our work was supported by the KIT as part of the HGF within the research program Earth & Environment: Changing Earth–Sustaining our Future.

Disclosures. The authors declare no conflicts of interest.

Data availability. Data underlying the results presented in this paper are not available to the public but maybe obtained from the authors upon reasonable request.

REFERENCES

1. F. Moulton, "Ti-doped sapphire: tunable solid-state laser," Opt. News **8**(6), 9 (1982).
2. Y. A. Carts, "Titanium sapphire's star rises," Laser Focus World **9**, 73–86 (1989).
3. R. L. Aggarwal, A. Sanchez, M. M. Stuppi, R. E. Fahey, A. J. Strauss, W. R. Rapoport, and C. P. Khattak, "Residual infrared absorption in as-grown and annealed crystals of Ti:Al_2O_3," IEEE J. Quantum Electron. **24**, 1003–1008 (1988).
4. L. DeShazer and J. Eggleston, "Extended infrared operation of titanium sapphire laser," *Conference on Lasers and Electro-Optics (CLEO)*, Baltimore, Maryland, 1987.

5. P. F. Moulton, "Spectroscopic and laser characteristics of Ti:Al_2O_3," J. Opt. Soc. Am. B **3**, 125–133 (1986).
6. R. Esterowitz, L. Allen, and C. P. Khattak, "Stimulated emission from flashpumped Ti:Al_2O_3," in *Tunable Solid State Lasers*, P. Hammerling, A. B. Budgor, and A. Pinto, eds. (Springer, 1985), pp. 73–75.
7. K. Gürel, V. J. Wittwer, M. Hoffmann, C. J. Saraceno, S. Hakobyan, B. Resan, A. Rohrbacher, K. Weingarten, S. Schilt, and T. Südmeyer, "Green-diode-pumped femtosecond Ti:sapphire laser with up to 450 mw average power," Opt. Express **23**, 30043–30048 (2015).
8. P. Pichon, A. Barbet, J.-P. Blanchot, F. Druon, F. Balembois, and P. Georges, "Light-emitting diodes: a new paradigm for Ti:sapphire pumping," Optica **5**, 1236–1239 (2018).
9. A. Hoffstädt, "Design and performance of a high-average-power flashlamp-pumped Ti:sapphire laser and amplifier," IEEE J. Quantum Electron. **33**, 1850–1863 (1997).
10. H. Vogelmann and T. Trickl, "Wide range sounding of free tropospheric water vapor with a differential absorption lidar (DIAL) at a high altitude station," Appl. Opt. **47**, 2116–2132 (2008).
11. H. Vogelmann, R. Sussmann, T. Trickl, and T. Borsdorff, "Intercomparison of atmospheric water vapor soundings from the differential absorption lidar (DIAL) and the solar FTIR system on Mt. Zugspitze," Atmos. Meas. Tech. **4**, 835–841 (2011).
12. T. Trickl, H. Giehl, H. Jäger, and H. Vogelmann, "35 yr of stratospheric aerosol measurements at Garmisch-Partenkirchen: from Fuego to Eyjafjallajökull, and beyond," Atmos. Chem. Phys. **13**, 5205–5225 (2013).
13. T. Trickl, H. Vogelmann, H. Giehl, H.-E. Scheel, M. Sprenger, and A. Stohl, "How stratospheric are deep stratospheric intrusions?" Atmos. Chem. Phys. **14**, 9941–9961 (2014).
14. T. Trickl, H. Vogelmann, H. Flentje, and L. Ries, "Stratospheric ozone in boreal fire plumes–the 2013 smoke season over central Europe," Atmos. Chem. Phys. **15**, 9631–9649 (2015).
15. H. Vogelmann, R. Sussmann, T. Trickl, and A. Reichert, "Spatiotemporal variability of water vapor investigated using lidar and FTIR vertical soundings above the Zugspitze," Atmos. Chem. Phys. **15**, 3135–3148 (2015).
16. T. Trickl, H. Vogelmann, A. Fix, A. Schäfler, M. Wirth, B. Calpini, G. Levrat, G. Romanens, A. Apituley, K. M. Wilson, R. Begbie, J. Reichardt, H. Vömel, and M. Sprenger, "How stratospheric are deep stratospheric intrusions? LUAMI 2008," Atmos. Chem. Phys. **16**, 8791–8815 (2016).
17. T. Trickl, H. Vogelmann, L. Ries, and M. Sprenger, "Very high stratospheric influence observed in the free troposphere over the northern Alps–just a local phenomenon?" Atmos. Chem. Phys. **20**, 243–266 (2020).
18. L. G. DeShazer, J. M. Eggleston, and K. W. Kangas, "Amplifier performance of Ti:sapphire," in *Advanced Solid State Lasers* (Optica Publishing Group, 1986), paper ThA10.
19. G. T. Maker and A. I. Ferguson, "Ti:sapphire laser pumped by a frequency-doubled diode-pumped Nd:YLF laser," Opt. Lett. **15**, 375–377 (1990).
20. T. R. Steele, D. C. Gerstenberger, A. Drobshoff, and R. W. Wallace, "Broadly tunable high-power operation of an all-solid-state titanium-doped sapphire laser system," Opt. Lett. **16**, 399–401 (1991).
21. G. Malcolm and A. Ferguson, "Ti:sapphire laser pumped by a frequency doubled diode pumped Nd:YLF laser," Opt. Commun. **82**, 299–304 (1991).
22. S. M. Spuler, K. S. Repasky, B. Morley, D. Moen, M. Hayman, and A. R. Nehrir, "Field-deployable diode-laser-based differential absorption lidar (DIAL) for profiling water vapor," Atmos. Meas. Tech. **8**, 1073–1087 (2015).
23. F. Späth, A. Behrendt, S. K. Muppa, S. Metzendorf, A. Riede, and V. Wulfmeyer, "3-D water vapor field in the atmospheric boundary layer observed with scanning differential absorption lidar," Atmos. Meas. Tech. **9**, 1701–1720 (2016).
24. M. Wirth, A. Fix, G. Ehret, J. Reichardt, R. Begie, D. Engelbart, H. Vömel, B. Calpini, G. Romanens, A. Apituley, K. M. Wilson, H. Vogelmann, and T. Trickl, "Intercomparison of airborne water vapour DIAL measurements with ground based remote sensing and radiosondes within the framework of LUAMI 2008," in *Proceedings of the 8th International Symposium on Tropospheric Profiling*, A. Apituley, H. Russchenberg, and W. Monna, eds. (2009). Poster presentation.
25. S. Ismail and E. V. Browell, "Airborne and spaceborne lidar measurements of H_2O profiles: a sensitivity analysis," Appl. Opt. **28**, 3603–3615 (1989).
26. S. Metzendorf, A. Behrendt, F. Späth, and V. Wulfmeyer, "High-power laser transmitter of the UHOH water vapor dial," in *The 28th International Laser Radar Conference (ILRC 28)*, Bucharest, Romania, June 25–30, 2017 . Oral presentation.
27. S. Metzendorf, "10 W-average-power single-frequency Ti:sapphire laser with tuning agility," Ph.D. thesis (University Hohenheim, 2018) (English).
28. G. Poberaj, A. Fix, A. Assion, M. Wirth, C. Kiemle, and G. Ehret, "Airborne all-solid-state dial for water vapour measurements in the tropopause region: system description and assessment of accuracy," Appl. Phys. B **75**, 165–172 (2002).
29. C. Kiemle, M. Wirth, A. Fix, G. Ehret, U. Schumann, T. Gardiner, C. Schiller, N. Sitnikov, and G. Stiller, "First airborne water vapor lidar measurements in the tropical upper troposphere and mid-latitudes lower stratosphere: accuracy evaluation and intercomparisons with other instruments," Atmos. Chem. Phys. **8**, 5245–5261 (2008).
30. M. Wirth, A. Fix, P. Mahnke, H. Schwarzer, F. Schrandt, and G. Ehret, "The airborne multi-wavelength water vapor differential absorption lidar WALES: system design and performance," Appl. Phys. B **96**, 201–213 (2009).
31. J. F. Pinto, L. Esterowitz, G. H. Rosenblatt, M. Kokta, and D. Peressini, "Improved Ti:sapphire laser performance with new high figure of merit crystals," IEEE J. Quantum Electron. **30**, 2612–2616 (1994).
32. D. S. Bethune, "Dye cell design for high-power low-divergence excimer-pumped dye lasers," Appl. Opt. **20**, 1897–1899 (1981).
33. E. Cromwell, T. Trickl, Y. Lee, and A. Kung, "Ultranarrow bandwidth VUV-XUV laser system," Rev. Sci. Instrum. **60**, 2888–2892 (1989).
34. T. Trickl, A. H. Kung, and Y. T. Lee, "Krypton atom and testing the limits of extreme-ultraviolet tunable-laser spectroscopy," Phys. Rev. A **75**, 022501 (2007).
35. A. Ogino, M. Katsuragawa, and K. Hakuta, "Single-frequency injection seeded pulsed Ti:Al_2O_3 ring laser," Jpn. J. Appl. Phys. **36**, 5112–5115 (1997).
36. K. Ertel, H. Linné, and J. Bösenberg, "Injection-seeded pulsed Ti:sapphire laser with novel stabilization scheme and capability of dual-wavelength operation," Appl. Opt. **44**, 5120–5126 (2005).
37. X. Baillard, A. Gauguet, S. Blze, P. Lemonde, P. Laurent, A. Clairon, and P. Rosenbusch, "Interference-filter-stabilized external-cavity diode lasers," Opt. Commun. **266**, 609–613 (2006).
38. M. G. Littman and H. J. Metcalf, "Spectrally narrow pulsed dye laser without beam expander," Appl. Opt. **17**, 2224–2227 (1978).
39. J. Bösenberg, "Ground-based differential absorption lidar for water-vapor and temperature profiling: methodology," Appl. Opt. **37**, 3845–3860 (1998).
40. P. L. Ponsardin and E. V. Browell, "Measurements of $H_2{}^{16}O$ linestrengths an air-induced broadenings and shifts in the 815 nm spectral region," J. Mol. Spectrosc. **185**, 58–70 (1997).
41. B. J. Butterworth, A. R. Desai, P. A. Townsend, *et al.*, "Connecting land–atmosphere interactions to surface heterogeneity in CHEESEHEAD19," Bull. Am. Meteorol. Soc. **102**(2), E421–E445 (2021).
42. S. Wiesner, "FESSTVaL (Field Experiment on Submesoscale Spatio-temporal Variability in Lindenberg)," 2021https://fesstval.de/.